

Extraction of Intrinsic Fluorescence in Fluorescence Imaging of Turbid Tissues

Gennadi Saiko¹ ^a and Alexandre Douplik² ^b

¹Swift Medical Inc, 1 Richmond St W, Toronto, Canada

²Department of Physics, Ryerson University, Toronto, Canada

Keywords: Fluorescence, Fluorescence Imaging, Intrinsic Fluorescence, Turbid Tissues.

Abstract: Interpretation of tissue fluorescence spectra can be complicated due to interplay with tissue optics. We have developed a photon propagation approach for correction of fluorescence on absorption in two realistic scenarios: when fluorophores are located a) on the surface of the turbid tissue and b) in a layer inside the turbid tissue. The approach takes into account the diffuse reflection of the tissue at excitation and emission wavelengths and does not require any precise measurement of optical properties (e.g., coefficient of absorption). The approach can be implemented using an inexpensive imaging setup and can be used in any setting.

1 INTRODUCTION

Fluorescence imaging is an important optical clinical modality and has numerous applications in diagnostics and surgical guidance.

Advances in clinical fluorescence imaging are related mostly to fluorescence angiography, which is based on the injection of a fluorescent dye in the bloodstream and subsequent visualization of blood vessels. Initially, the method was developed for ophthalmology using fluorescein as the dye (e.g., Intravenous Fluorescein Angiography (IVFA) or Fluorescent Angiography (FAG) for examining the circulation of the retina and choroid).

Recently, the method has been extended to other blood vessels using Indocyanine green (ICG), which is a non-toxic, protein-bound dye that is retained within the vasculature after intravenous injection for several minutes until rapid clearance by the liver (Sevick-Muraca, 2012).

Endogenous fluorescence in tissues is associated with tissues' autofluorescence and bacterial (or fungal) presence.


Autofluorescence in turbid tissues is attributed mainly to proteins, collagen, and elastin. Collagen (or elastin in other tissues) is the major contributor to the

tissue autofluorescence; it is accountable for up to 95% of fluorescence in visible spectra. Collagen/elastin is excited in the range of 370-450 nm and re-emits in the range 490-580 nm.

Some interesting possibilities are connected with other tissue fluorophores, including the reduced form of coenzyme nicotinamide adenine dinucleotide (NADH), which is sensitive to tissue oxygen concentration.

Bacteria fluorescence can be particularly important in wound care to a) identify particular strains in the wound, b) assess (qualitatively or quantitatively) bacteria presence, or c) guide sampling, debridement, or antimicrobial selection. All wounds contain bacteria (e.g., *Staphylococcus*, *Streptococcus*, *Pseudomonas* species, and *Coliform* bacteria), at levels ranging from contamination through critical colonization to infection. Most of the clinically important strains (both gram-positive and negative) clearly show a distinctive double-peak of tryptophan fluorescence (Dartnell, 2013). Unfortunately, these bands are within the UVC band, which makes it problematic for clinical use. However, some clinically relevant bacteria (*S. aureus*, *S. epidermidis*, *Candida*, *S. marcescens*, *Viridans streptococci*, *Corynebacterium diphtheriae*, *S. pyogenes*, *Enterobacter*, and *Enterococcus*) produces

^a  <https://orcid.org/0000-0002-5697-7609>

^b  <https://orcid.org/0000-0001-9948-9472>

red fluorescence (Kjeldstad, 1985), while *P. aeruginosa* produced a bluish-green fluorescence (Cody, 1987).

Interpretation of tissue fluorescence spectra could be complicated due to interplay with tissue optics. Thus, fluorescence spectra measured *in vivo* can be significantly different from those from pure fluorophores in lab conditions.

Several approaches to deal with this problem have been developed in recent years. Comprehensive review of correction techniques was performed by Bradley et al (Bradley, 2006). They classified these techniques into four broad groups: empirical techniques, measurement-method based techniques, theory based techniques, and Monte Carlo based techniques. In particular, some groups (Liu 1992, Anidjar 1996) used spectroscopy at several wavelengths (e.g., their ratio) to take into account absorption. Other groups attempted to retrieve intrinsic fluorescence spectra from raw fluorescence spectra measured in biological tissues. In particular, Wu et al. (Wu, 1993) developed a photon migration model to extract intrinsic fluorescence in turbid media. An amended photon migration model was proposed by Muller et al. (Muller, 2001). Pfefer et al. (Pfefer, 2001) used Monte Carlo simulations to analyze the effect of optical fiber diameter, distance to tissue, and numerical aperture on light propagation during fluorescence spectroscopy with a single-fiber probe. Kim et al. (Kim, 2010) proposed an elegant model to quantify *in vivo* fluorescence in spatially resolved fiber optic measurements. Valdes et al. (Valdes, 2017) successfully applied Kim's model to retrieve intrinsic fluorescence in an imaging modality. Yang et al. (Yang, 2014) applied structured light to decrease the influence of absorption on fluorescence imaging. Lin et al. (Lin, 2001) compared fluorescence and reflection spectra to reduce spectral distortions caused by superficial blood contamination on tissue optical spectra during surgical operations (resections). More recently Zhang et al (Zhang, 2018) used particle swarm optimization algorithm in combination with a optic fiber probe to extract intrinsic tissue fluorescence spectrum.

However, existing models suffer from several shortcomings, which complicate their translation into clinical imaging applications. Namely, some of them (e.g., Pfefer, 2001) were developed for a particular collection geometry (e.g, a single fiber or multi-fiber geometry), which are quite different from imaging geometries. Other (e.g., Kim, 2010) require accurate measurements of optical tissue parameters (e.g., the absorption coefficient), which can be impractical in non-hospital applications.

The purpose of this article is to develop an approach, which can deconvolute intrinsic fluorescence in typical tissue imaging geometry without precise measurements of optical tissue parameters. Such as fluorescence imaging has multiple applications in wound care, we will illustrate our approach with fluorophores produced by clinically relevant bacteria (*P.aeruginosa* and *S.aureus*). It is a particularly complicated case, because these fluorophores (pyoverdine and porphyrins, respectively) have absorption peaks in the same range (400nm) as hemoglobins.

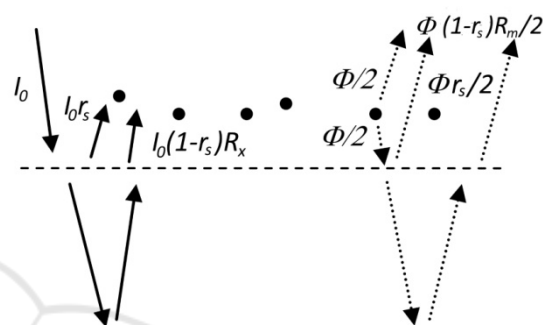


Figure 1: Contributions to the excitation flux (left side, solid lines) and the emission flux (right side, dotted lines) if fluorophores are located above the surface.

The article is structured as follows:

First, we develop a photon propagation approach to calculate the fluorescence if fluorophores are located on the surface of the tissue. For this, we consider excitation and emission photons separately.

Then, we will use a similar photon propagation approach to calculate the fluorescence if fluorophores are located inside the tissue.

2 THEORY

In realistic conditions, biological fluorophores are typically located inside the tissue (e.g., collagen). However, in some cases, fluorophores can be located on the surface of the tissue (e.g., bacteria and fungi during contamination and colonization stages). So, to elucidate the differences between these two cases, we consider them separately.

2.1 Fluorophores on the Surface

Let's consider fluorophores that are located on the surface of the tissue.

The fluorescence output (flux, W/m^2) Φ is proportional to the surface density of fluorophores n , their absorption cross-section σ and quantum yield ϕ , and an excitation flux I_x .

$$\Phi = n\sigma\phi I_x = f I_x \quad (1)$$

here f is an intrinsic fluorescence.

The excitation flux I_x (see Figure 1), consists of an inbound directional flux I_0 (illumination) and outbound directional flux I_r , which was reflected from the tissue. The outbound flux I_r consists of two components: specular reflection I_s and diffuse reflectance I_d . If we assume that the absorption on the surface is small, then we can write

$$I_x = I_0 + I_s + I_d = I_0(1 + r_s + (1 - r_s)R_x) \quad (2)$$

here, r_s is the coefficient of specular reflection ($r_s = (n - 1)^2 / (n + 1)^2$, where n is the relative index of refraction), and R_x is the coefficient of diffuse reflectance of the tissue at an excitation wavelength.

The fluorophores re-emit isotropically in all directions (see Figure 1). Thus, $1/2$ of the output goes into the upper hemisphere and can be immediately collected by the imaging system. The other half of the fluorescence output will shine into the lower hemisphere. A minor part of it will be immediately reflected by the surface (specular reflection), while the major part will go into the tissue, and some of them will be reflected through diffuse reflectance. Thus, the measured fluorescence can be written as

$$F = \Phi/2(1 + r_s + (1 - r_s)R_m) \quad (3)$$

here, R_m is the coefficient of diffuse reflectance of the tissue at an emission wavelength.

It should be noted that (3) assumes that we can collect all photons emitted in the upper hemisphere, which is not true in any realistic imaging scenario. A realistic fluorescence signal will contain a geometric factor, which takes into account a collection geometry (e.g., numeric aperture). However, such as the collection geometry stays constant in the experiment we will ignore this geometric factor in our calculations.

Then, the intrinsic fluorescence f can be expressed as

$$f = \frac{2F}{I_0} \frac{1}{(1 + r_s + (1 - r_s)R_m)} \quad (4)$$

$$* \frac{1}{(1 + r_s + (1 - r_s)R_x)}$$

Thus, the correction factor contains the coefficient of specular reflection and coefficients of tissue reflectance at excitation and emission wavelengths.

2.2 Fluorophores in the Tissue

The more realistic fluorescence imaging scenario is when fluorophores are located in the tissue. It can be collagen, which is localized mostly in the dermis, siderophores, or metabolic by products produced by bacteria in the epidermis (impetigo), dermis (folliculitis, erysipelas), subcutaneous fat (cellulitis) or fascia (necrotic fasciitis). It can be noted that in all of the mentioned above cases, the fluorophores are localized in a layer (e.g., collagen in interstitial tissue), rather homogeneously distributed across depth. Based on this observation, the following model can be considered: the fluorophores are located in a thin layer parallel to the tissue surface. In this case we can ignore the heterogeneity of excitation light distribution within this layer.

To calculate the fluorescence signal, we can take the following approach: 1) calculate the excitation flow in the tissue, 2) multiply it by the intrinsic fluorescence, and 3) take into account reflection and scattering of the emission flux within the tissue using emission photon propagation model.

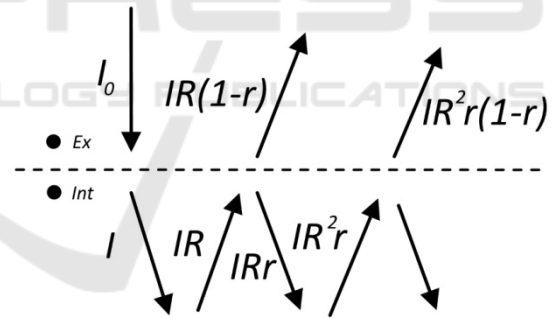


Figure 2: Contributions to the excitation flux.

The fluorophores absorb photons from the incoming (e.g. collimated) flow. However, in addition to the incoming flow, they will be excited by a flow of diffusively reflected photons. Their steady-state distribution will be greatly impacted by the optical properties of the tissue and particularly by mismatched boundary conditions. To take into account that diffuse flow we can consider the following simplified model. Let's consider two points in the close vicinity of the interface: one is slightly above, one is slightly below the surface (see Figure 2). We can roughly calculate the flow in each of these points using the following considerations. Let's assume that the incoming flux in the tissue is I ($I =$

$I_0(1 - r_s)$). The inbound flux has the probability R (bulk tissue reflectance) to be diffusively reflected. Thus, the diffusively reflected flow (outbound flux) near the surface will be IR . Now, on the surface, the light can be reflected with the probability r (specular reflection coefficient, which depends solely on the relative index of refraction) or escape the tissue with probability $1-r$. And this process is repeated indefinitely.

Thus, the flow just below the surface can be calculated as

$$I_{int} = I + IR + IRr + IR^2r + \dots \quad (5)$$

$$= \frac{I}{1 - Rr} + \frac{IR}{1 - Rr}$$

The flow just above the surface can be calculated as

$$I_{ex} = IR(1 - r) + IR^2r(1 - r) + \dots \quad (6)$$

$$= \frac{IR(1 - r)}{1 - Rr}$$

From (6) one can see that $I_{ex} = IR_d$, where

$$R_d = \frac{R(1 - r)}{1 - Rr} \quad (7)$$

is the diffuse reflectance of the tissue, which can be measured experimentally.

According to (5), the flow just below the surface is γ times larger than the initial inbound flow I ($I_{int} = \gamma I$), where

$$\gamma = \frac{1 + R}{1 - Rr} \quad (8)$$

Such as the probability R is unknown, we can express it using diffuse reflectance R_d , which can be measured experimentally and r , which can be assessed analytically or numerically. Resolving (7) over R and substituting it into (8) gives us

$$\gamma = 1 + R_d + \frac{2rR_d}{1 - r} \quad (9)$$

Specular reflection coefficient r can be found using Fresnel theory and assumptions about angular light distribution below the surface (Welch, 2011). The simplified diffuse approximation model (Star, 2011) provides a good estimate for that value; $r = 1 - n^{-2}$, where n is the relative index of refraction. In this case, (9) can be rewritten as

$$\gamma \sim 1 + (2n^2 - 1)R_d \quad (9')$$

For a realistic index of refraction $n=1.41$, one can see that $\gamma \sim 1 + 3R_d$, which is in a reasonable agreement with estimates based on diffuse approximation theory (Star, 2011).

Now, let's turn to the fluorescence. Excitation photons propagate through a thin fluorescent layer in a ballistic way. Thus, the probability of getting absorbed is $n\sigma = Nl\sigma$, where N is the volume concentration of fluorophores, l is the thickness of their layer. Then, the fluorophores re-emit light with probability ϕ (quantum yield) isotropically in all directions (see Figure 3).

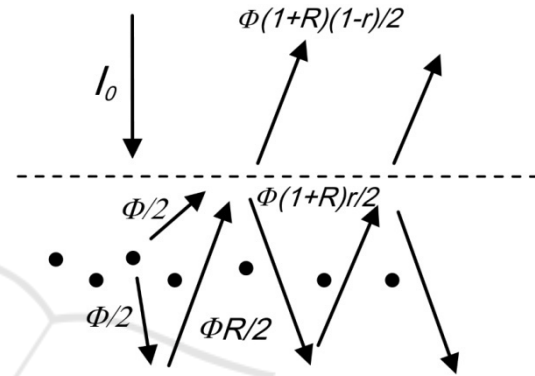


Figure 3: Contributions to the emission flux if fluorophores are located below the surface.

Thus, $1/2$ of the output is emitted in the upper hemisphere. The other half of the fluorescence output will shine in the lower hemisphere, and some of these photons will be reflected through diffuse reflectance with probability R . Similarly to (6), if we take into account the probability of specular reflection on the tissue/air interface r , then the measured fluorescence can be calculated as

$$F = \Phi(1 + R)(1 - r)/2 + \Phi(1 + R)Rr(1 - r)/2 + \dots = \frac{\Phi(1 + R)(1 - r)}{2(1 - Rr)} \quad (10)$$

One can see that a multiplier in (10) is equal to $\gamma(1 - r)$. Thus, using (9) this expression can be rewritten as:

$$F = \frac{\Phi}{2}(1 + R_d - r + R_d r) \quad (11)$$

here, R_d should be measured at the emission wavelength (R_m). If we use $r = 1 - n^{-2}$ approximation, then

$$F \sim \frac{\Phi}{2n^2} (1 + (2n^2 - 1)R_d) \quad (11')$$

We need to mention here that the diffuse reflectance in expression (11) and (11') are at emission wavelength.

So, if we insert R_x and R_m for diffuse reflectance at excitation and emission wavelengths, then the final expression for the intrinsic fluorescence will be

$$f = \frac{2F}{I_0(1 - r_s)} \frac{1}{(1 + R_m - r + R_m r)} \quad (12)$$

$$* \frac{1}{(1 + R_x + \frac{2rR_x}{1-r})}$$

If we use $r = 1 - n^{-2}$ approximation, then

$$f \sim \frac{2F}{I_0(1 - r_s)} \frac{n^2}{(1 + (2n^2 - 1)R_m)} \quad (12')$$

$$* \frac{1}{(1 + (2n^2 - 1)R_x)}$$

For $n=1.41$ an approximate expression will be

$$f \sim \frac{F}{I_0} \frac{4}{(1 + 3R_m)(1 + 3R_x)} \quad (12'')$$

3 RESULTS

3.1 Fluorophores on the Surface

If we illuminate the tissue at some wavelength with intensity I_0 and measure its reflectance using the same imaging geometry, then for the smooth surface, the measured reflectance signal will be $I_0(1 - r_s)R_d$

Thus, to implement the correction algorithm for fluorophores located on the absorbing surface, the following steps can be taken:

1. Illuminate tissue at the excitation wavelength and measure R'_x ($R'_x = (1 - r_s)R_x$)
2. Illuminate tissue at an emission wavelength and measure R'_m ($R'_m = (1 - r_s)R_m$)
3. Measure or estimate r_s
4. Calculate R_x and R_m
5. Calculate the correction factor according to (4)

3.2 Fluorophores in the Tissue

Similarly, to implement the correction algorithm for fluorophores located inside the turbid tissue, the following steps can be taken:

1. Illuminate tissue at the excitation wavelength and measure R'_x ($R'_x = (1 - r_s)R_x$)
2. Illuminate tissue at an emission wavelength and measure R'_m ($R'_m = (1 - r_s)R_m$)
3. Measure or estimate the index of refraction n
4. Calculate r_s and r
5. Calculate R_x and R_m
6. Calculate the correction factor according to (12)

To illustrate the application of the developed model, we have calculated the correction factors as a function of R_x and R_m , for clinically relevant conditions (see Table 1). In particular, we consider excitation at 405nm and emission in 470nm range (*P.aeruginosa*) or 620nm range (*S.aureus*). In this case, one can expect $R_x=0.005-0.01$ and $R_m=0.12-0.18$ and 0.3-0.4, respectively.

Table 1: Estimated correction factor for pyoverdin and porphyrin fluorescence ($n=1.4$).

Excitation\Emission	470nm ($R_m=0.12-0.18$)	620nm ($R_m=0.3-0.4$)
405nm ($R_x=0.1$)	2.25-1.99	1.62-1.4

Besides, we have calculated sensitivities of the correction factor to the change in parameters n and R_m , S_n (see Figure 4), and S_{R_m} (see Figure 5), respectively. For example, the sensitivity to n (S_n) is equal to a change (in %) in the correction factor for a given change (in %) in n : $\Delta c/c = S_n \Delta n/n$.

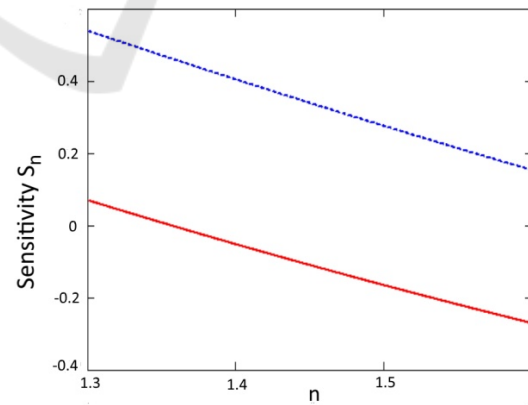


Figure 4: Sensitivity S_n as a function of the index of refraction n . Pyoverdine fluorescence ($R_x=0.1$, $R_m=0.2$) and porphyrin fluorescence ($R_x=0.1$, $R_m=0.4$) are depicted by dotted blue and solid red lines, respectively.

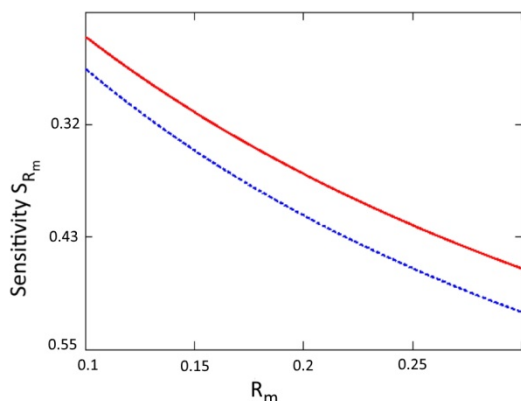


Figure 5: Sensitivity S_{R_m} as a function of the reflectance at emission wavelength R_m , for different indexes of refraction 1.4 (solid red line) and 1.5 (dotted blue line), respectively. R_x was set to 0.1.

4 DISCUSSION

We have obtained explicit equations for the correction factor if fluorophores are located on the surface of the tissue (equation (4)) and inside of the tissue (equation (12)).

We have found that to retrieve intrinsic fluorescence we need to know diffuse reflectance of tissue at excitation and emission wavelengths. It can be embedded into the imaging algorithm: 1) capture reflectance maps at excitation and emission wavelengths, 2) calculate the correction factor (per pixel), 3) apply the correction factor (per pixel) to retrieve intrinsic fluorescence.

From equations (4) and (12) one can see that the correction factors have approximately the same structure ($\frac{1}{(1+cR_x)(1+cR_m)}$) for fluorophores located above and below the surface of the tissue. The first operand (one) corresponds to the nonreflected flow (external illumination for excitation, and re-emission in the upper hemisphere for fluorescence), while the second operand corresponds to the reflected flow. The main difference is an amplification ($c>1$) of the optical flux near the border of the tissue with mismatched boundary conditions.

From equations (4) and (12), one can see that both the excitation component and emission component contribute to the correction factor similarly, which is quite different from Kim's model (Kim, 2010). We should note that they assumed a homogeneous distribution of fluorophores in the tissue, which is not always a realistic assumption.

From Figures 4 and 5, one can see that the correction factor is relatively insensitive to errors in

the determination of parameters n and R_m . For example, 0.05 error in the determination of the index of refraction (3.5%) will translate into less than 2% correction factor error. Likewise, 10% error in determination of the R_m will translate into 3-5% correction factor error. These results can simplify the correction algorithm by eliminating reflectance measurements at the excitation wavelength in some cases. If we consider 400nm range, such as the sensitivity is quite small (we can use Figure 5 as a proxy), then even a rough approximation of the diffuse reflectance ($\pm 50\%$ accuracy) will lead to 10-15% correction factor error. However, for more precise measurements, capturing R_x reflectance map can be helpful.

The coefficient of specular reflection r_s ($r_s = (n-1)^2/(n+1)^2$) varies insignificantly with the wavelength in UVA and visible spectra and stays within a 2-5% range for biologically relevant indexes of refraction ($n=1.3-1.6$). It is reasonable to assume that the index of refraction stays constant within one object, so it is not necessary to correct for it within one image. However, if more accurate quantification of fluorescence is required, then correction on specular reflection can be helpful.

In realistic imaging settings, the algorithm requires certain modifications. An imaging sensor typically integrates the light over a certain spectral range. If we take into account that the fluorescence is typically broadband, then to calculate the correction coefficient accurately, certain precautions have to be taken. Ideally, we can measure tissue reflectance at the whole fluorescence spectra range and then integrate (4) or (12) over that range. However, in the first approximation, we can measure tissue reflectance at fluorescence spectra maximum.

Finally, the proposed model assumes that the fluorophores form a thin layer within the tissue close to its surface. This assumption is valid if the thickness of the layer is significantly smaller than the effective penetration depth. For example, using optical parameters for the skin at 400nm $\mu_a = 3.76\text{cm}^{-1}$, and $\mu'_s = 71.8\text{cm}^{-1}$ (Bashkatov, 2011), we can find that $\mu_{eff} = 29.2\text{cm}^{-1}$. Thus, for layers with thickness $l = 300\mu\text{m}$ and below and located within 300mm from the surface (epidermis and upper dermis) that assumption holds.

In the future, we plan to validate our models in experiments on absorbing phantoms. In particular, we plan to use layered phantoms (Saiko, 2018) with an absorption layer (gelatine and hemoglobins) and a fluorescence layer (gelatine and quantum dots), stacked in a sandwich structure.

5 CONCLUSIONS

We have proposed a photon propagation model for correction of fluorescence on absorption in two realistic scenarios: when fluorophores are located a) on the surface of the turbid tissue and b) in a layer within the turbid tissue. The models require measurements of diffuse reflection of the tissue at excitation and emission wavelength and do not require precise measurement of optical properties (e.g., coefficient of absorption). The approach can be implemented using an inexpensive imaging setup and can be used in any setting.

REFERENCES

- Sevick-Muraca E.M., 2012, Translation of Near-Infrared Fluorescence Imaging Technologies: Emerging Clinical Applications, *An Rev Med*, 63: 217-231.
- Dartnell L.R., Roberts T.A., Moore G., Ward J.M., Muller J.P., 2013. Fluorescence Characterization of Clinically-Important Bacteria. *PLoS ONE*; 8: e75270.
- Kjeldstad B, Christensen T, Johnsson A. 1985. Porphyrin photosensitization of bacteria. *Adv. Exp. Med. Biol.* 193: 155-159.
- Cody Y.S, Gross D.C. 1987. Characterization of pyoverdinin (pss), the fluorescent siderophore produced by *Pseudomonas syringae* pv. *Syringae*. *Appl. Environ. Microbiol.* 53: 928-934.
- Bradley R. S., Thorniley M. S., 2006, A review of attenuation correction techniques for tissue fluorescence. *J. Roy. Soc, Interface*, 3(6), 1–13.
- Liu C. H., Das B. B., Glassman W. L. S., Tang G. C., Yoo K. M., Zhu H. R., Akins D. L., Lubicz S. S., Cleary J., Prudente R., Celmer E., Caron A., and Alfano R. R., 1992. Raman, fluorescence, and time-resolved light-scattering as optical diagnostic-techniques to separate diseased and normal biomedical media, *J. Photochem. Photobiol. B* 16-2 187–209.
- Anidjar M., Cussenot O., Avrillier S, Etori D., Villette M. J., Fiet J., Teillac P., and Le Duc A., 1996. Ultraviolet laser-induced autofluorescence distinction between malignant and normal urothelial cells and tissues, *JBO*. 1, 335–341.
- Wu J., Feld M. S., and Rava R. P., 1993. Analytical model for extracting quantitative fluorescence in turbid media, *Appl. Opt.* 32, 3585–3595.
- Muller M. G., Georgakoudi I., Zhang Q., Wu J., and Feld M. S., 2001. Intrinsic fluorescence spectroscopy in turbid media: disentangling effects of scattering and absorption, *Appl. Opt.* 40, 4633–4646.
- Pfeifer T. J., Schomacker K. T, Ediger M. N, and Nishioka N. S., 2001. Light propagation in tissue during fluorescence spectroscopy with single-fiber probes, *IEEE J. Sel. Top. Quantum Electron.* 7, 1004–1012.
- Kim A., Khurana M., Moriyama Y., and Wilson B. C., 2010. Quantification of in vivo fluorescence decoupled from the effects of tissue optical properties using fiber-optic spectroscopy measurements, *JBO*. 15(6), 067006.
- Valdes P.A., Angelo J.P., Choi H.S, and Gioux S, 2017. qFSSOP: real-time optical property corrected fluorescence imaging, *BOE* 8, 3597-3605.
- Yang B., Tunnell J.B., 2014. Real-time absorption reduced surface fluorescence imaging, *JBO*, 19(9), 090505.
- Lin W.C, Toms S.A, Jansen E.D, and Mahadevan-Jansen A, 2001. Interoperative Application of Optical Spectroscopy in the Presence of Blood, *IEEE J. on Sel. Top. in Quantum Electron.*, 7(6), 996- 1003.
- Zhang Y., Hou H., Zhang Y., Wang Y., Zhu L., Dong M., Liu Y., 2018, Tissue intrinsic fluorescence recovering by an empirical approach based on the PSO algorithm and its application in type 2 diabetes screening, *BOE* 9: 1795-1808.
- Welch A.J., van Gemert M.J.C., Star W.M., 2011, Definitions and Overview of Tissue Optics in *Optical-Thermal Response to Laser-Irradiated Tissue*, Ed. Welch AJ, Springer, Dordrecht, NLD, 2nd edition.
- Star W.M., 2011, Diffuse Theory of Light Transport in *Optical-Thermal Response to Laser-Irradiated Tissue*, Ed. Welch AJ, Springer, Dordrecht, NLD, 2nd edition.
- Bashkatov A.N., Genina E.A., Tuchin V.V, 2011. Optical Properties of Skin, Subcutaneous, and Muscle Tissues: a Review, *J. Inn. Opt. Health Sci*, 4(1) 9-38.
- Saiko G., Zheng X., Betlen A., Douplik A., 2019, Fabrication and Optical Characterization of Gelatin-Based Phantoms for Tissue Oximetry, *Adv Exp Med Biol* (in press).